First-principles study of bilayer polymeric manganese phthalocyanine

Haechan Park, Shuanglong Liu, James N. Fry, and Hai-Ping Cheng

Phys. Rev. B **105**, 195408 — Published 5 May 2022

DOI: 10.1103/PhysRevB.105.195408

A First-Principles Study of Bilayer Polymeric Manganese Phthalocyanine

Haechan Park[1,2], Shuanglong Liu[1,2], James N. Fry,[1], and Hai-Ping Cheng[1,2*]
[1] *Department of Physics, University of Florida, Gainesville, Florida 32611, USA*
[2] *Quantum Theory Project and Center for Molecular Magnetic Quantum Materials, University of Florida, Gainesville, Florida 32611, USA*
(Dated: March 18, 2022)

We study bilayer manganese phthalocyanine (MnPc) molecules and MnPc polymeric sheets using first-principles simulations, with a focus on the magnetic interactions between Mn atoms. We find that the most stable position of the upper layer with respect to the lower layer is shifted about 1/8 of a lattice vector from the center of the bottom layer along the direction toward a nearest-neighbor N atom. The magnetic ground state is the Néel anti-ferromagnetic (NAF) configuration within a layer and ferromagnetic between Mn atoms in adjacent layers. In this state, the system becomes a semiconductor with an indirect band gap of 11 meV. The strongest interaction is the interlayer coupling between the closest Mn atoms. A maximally-localized Wannier analysis suggests that the dominant coupling pathway is Mn-(N,C)-Mn rather than a direct Mn-Mn coupling. The maximum calculated magnetic anisotropy energy is found to be 1.0 meV per Mn atom. We also find that the bilayer molecule shows a significant stacking angle change from FM to AFM configurations accompanied by a change of orbital filling ordering.

I. INTRODUCTION

Interest in two-dimensional (2D) materials arises from possible novel electronic properties because of their ultra thin structure leading to quantum confinement in one of the three dimensions, with prospective applications in electronics. Many 2D systems are considered as programmable materials. For example, graphene is a semimetal with remarkably high electron mobility [1], whereas phosphorene and transition metal dichalcongenides are outstanding for band gap tunabilty [2, 3] and valleytronics [4, 5], respectively. Since 2015, there has also been a surge in the study of 2D magnetism [6, 7] for potential applications in information storage [8–11] and spintronic devices [12]. Some 2D magnetic materials exhibits enhanced spin fluctuations, adding yet more intensity to the field [13, 14]. Intrinsically ferromagnetic (FM) materials are desirable as a building block for practical devices. Many 2D materials have been found to be ferromagnetic, such as CrI_3 and $Cr_2Ge_2Te_6$ as well as materials that are ferromagnetic even at room temperatures [15–18]. Some of these materials show layer dependent magnetism. For $Cr_2Ge_2Te_6$ thin layers, a FM transition depends on the number of layers [19]. In CrI_3 thin films, a monolayer shows FM behavior, while a bilayer presents anti-ferromagnetic (AFM) behavior and a trilayer reverts to FM [20]. Controllability of magnetic phases by an electric field is also demonstrated in CrI_3 [14].

Another class of 2D magnetic materials that is worth more attention is the molecular based magnetic 2D network. The most recently synthesized molecular 2D system is the $[Fe(tBu_2qsal)_2]$ spin crossover mononuclear complex [21]. Between 117–119 K, the layered bulk material system shows a hysteretic spin transition from low-spin (LS, ground state, zero spin) to high-spin (HS, spin equal to 1) states. Capacitance measurements are performed over a thin film junction device that demonstrates clearly a difference between the LS and HS states. Characterization of mono-, bi-, and few-layer systems is ongoing (private communication) and the full potential of this new 2D material is yet to be unveiled. A more commonly known molecular network is the metal-phthalocyanine (MPc) system, also classified as metal-organic framework (MOF), which typically consists of a transition metal atom at the center surrounded by an organic framework, for example, phthalocyanine. In MPc, the transition metal ion holds a local spin magnetic moment whose value depends on the specific element. This gives it advantages in tunable electronic and magnetic properties by cation substitution [22–25]. One of the applications of MPc molecules is to control field-effect transistor characteristics made from 2D transistion metal dichalcogenides (TMDs) [26]. In physisorbed MPc with different metal ions on TDMs, one can *n*-dope or *p*-dope TMDs. MPc molecules can also stack into chain configuration to form 1D spin chains [27, 28], which maybe be useful for quantum information science.

MnPc molecules also show interesting physics in interactions with substrates. For example, it has been demonstrated that a highly spin-polarized interface, also known as spinterface [30, 31], can be formed between MnPc and a Co substrate. [32] Long-range magnetic ordering via an Au substrate between MnPc and iron phtalocyanine (FePc) has been realized [33]. In the bulk form of MPc, the molecules are bonded by a Van der Waals force making it a 2D molecular crystal. Depending on the stacking angle, which will be discussed in more detail in a later section, the magnetic properties change [29, 34]. There also exist polymeric MnPc (poly-MnPc) monolayers that have been synthesized by Koudia *et al.* [23], although the size of the poly-MnPc monolayer is only 10 nm × 10 nm. We note that MnPc molecules are bonded covalently within a poly-MnPc monolayer. Wang *et al.* [25] studied mono-

* hping@ufl.edu

layer poly-MnPc, revealing their magnetism and a magnetic phase transition due to electrostatic gating. Despite much research on molecular MnPc films, it is unclear how poly-MnPc films stack and interact in terms of magnetism and electronic structure, which is essential information for these materials to be promising candidates as building blocks of molecular electronics/spintronics devices.

Motivated by the fundamental understanding of magnetic interactions in molecular magnetic systems, this work focuses on the stacking pattern and magnetic coupling in manganese phthalocyanine (MnPc). Previous work has reported magnetic interactions in bulk form [29]. In this study, we investigate structural, electronic, and magnetic properties of bilayer polymeric and molecular MnPc based on first-principles simulations within Kohn-Sham density functional theory (DFT). [35, 36] We report low-energy interlayer stackings and the magnetic configuration in the ground state for bilayer poly-MnPc. Exchange coupling parameters are fit to a classical spin Hamiltonian for the most stable bilayer poly-MnPc with DFT total energies in different magnetic configurations, followed by our analysis of magnetic coupling pathways in the bilayer poly-MnPc with the aid of Wannier functions. Lastly, a comparison between polymeric and molecular forms is discussed.

II. COMPUTATIONAL METHOD

Our calculations are based on spin-dependent DFT as implemented in the Vienna Ab Initio Simulation Package (VASP) [37, 38]. We set the energy cutoff for plane waves to be 450 eV. We sampled the reciprocal space by a $9 \times 9 \times 1$ ($4 \times 4 \times 1$) Monkhorst-Pack k-point mesh [39] for 1×1 unit cells of bilayer polymeric (molecular) MnPc. For 2×2 supercells of bilayer poly-MnPc, we sampled the reciprocal space by a $5 \times 5 \times 1$ Monkhorst-Pack k-point mesh. We adopted the exchange correlation energy functional optB86b proposed by Klimes *et al.* [40] to include van der Waals interactions between two MnPc layers and projector augmented wave (PAW) pseudopotentials [41]. We checked that the energy difference between the FM state and the AFM state is converged. The energy tolerance of electronic self-consistency and the force tolerance were set to 10^{-5} eV and 0.02 eV/Å respectively for the stable stacking search. All other calculations use an energy tolerance of 10^{-8} eV and a force tolerance of 0.01 eV/Å. When using the DFT+U method [42] we applied $U = 4.0$ eV and $J = 1.0$ eV for Mn d orbitals to better describe the magnetic properties[25]. The DFT+U method was not used during ionic relaxation. We obtained maximally localized Wannier functions (WF) [43, 44] for the energy bands around the Fermi level using the Wannier90 package [45].

III. RESULTS AND DISCUSSION

A. Stable Interlayer Stacking

As shown in Fig. 1a, a single MPc molecule has in the center a transition metal atom M, which could be Mn, Fe, Co, Ni, Cu, *etc.* In Fig. 1a, we mark two nitrogen atoms by N1 and N2 respectively. N1 (N2) is one of the four pyrrole (azamethine) nitrogen atoms. Transition-metal-atom chains are formed in MPc molecular crystals and thin films when MPc molecules are stacked together. Various stackings are characterized by the angle θ between a metal chain and the plane of the molecule, as shown in Fig. 4b. Two stacking phases have been widely established in MPc materials, denoted α and β, where the α phase has $\theta \approx 65°$ and β has $\theta \approx 45°$ [18]. For the α phase, two sub-models of stacking have been proposed [18], the so-called $\alpha+$ model, where the stacking direction is along the line connecting the M-N1 line, and the $\alpha\times$ model, where the stacking is along the M-N2 line. It is noteworthy that in all of these three stackings there is no relative rotation about the normal of the MPc molecular plane . In the following, we examine stable stackings position in bilayer poly-MnPc and compare them with the above-mentioned stackings in MPc molecular crystals and thin films.

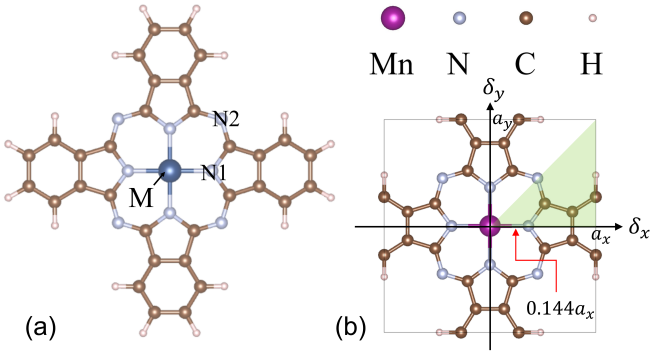

FIG. 1. Schematics of (a) a MPc molecule and (b) a unit cell of poly-MnPc monolayer.

Ignoring a rotation in the MnPc plane, we characterize the stacking in bilayer poly-MnPc by the relative in-plane shift $\boldsymbol{\delta} = \delta_x \boldsymbol{a}_x + \delta_y \boldsymbol{a}_y$ where $\boldsymbol{a}_{x/y}$ is the lattice vector in the x/y-direction (see Fig. 1b). For each relative shift, we constrain the x- and y-coordinates of Mn atoms and relax all the other degrees of freedom except the cell parameters, which are energetically optimal at zero relative shift. Afterward, we calculate the binding energy $E_\mathrm{b} = E_2 - 2E_1$, where E_2 and E_1 are the energies of bilayer poly-MnPc and monolayer poly-MnPc respectively. The bilayer poly-MnPc is always held in the ferromagnetic state to yield consistent binding energies. Given the four-fold rotational symmetry and a mirror-plane symmetry of monolayer poly-MnPc, it is sufficient to shift the top layer within 1/8 of the unit cell, $0 \le \delta_y \le \delta_x \le 1/2$, as highlighted in Fig. 1b.

Fig. 2a shows the binding energy E_b as a function of δ_x and δ_y. Stable stackings correspond to local minima of $E_\mathrm{b}(\delta_x, \delta_y)$. As seen from the figure, there are three stable stackings, at $(\delta_x, \delta_y) \approx (0.25, 0.25)$, $(0.5, 0.15)$, and $(0.15, 0.00)$. A careful search shows that the most stable stacking is of $\alpha+$ type with a stacking angle $\theta = 61.1°$ (see Fig. 2b). The next most stable stacking, 98 meV higher in energy, is of $\alpha\times$ type with $\theta = 40.2°$. The interlayer distance is about 3.17 Å for both $\alpha+$ and $\alpha\times$ stackings at their minimum energy angle. We determine the interlayer distance by averaging the z-coordinate of all atoms except Mn atoms, because a Mn atom in the top (bottom) layer lies below (above) the molecular plane by about 0.1 Å (see Fig. 4). Such a structural distortion is not present in monolayer poly-MnPc, and thus it is likely due to the asymmetrical chemical environment in the out-of-plane direction around each Mn atom. For the most stable stacking, we relax the lattice constants further and find $a_x = 10.640$ Å and $a_y = 10.638$ Å.

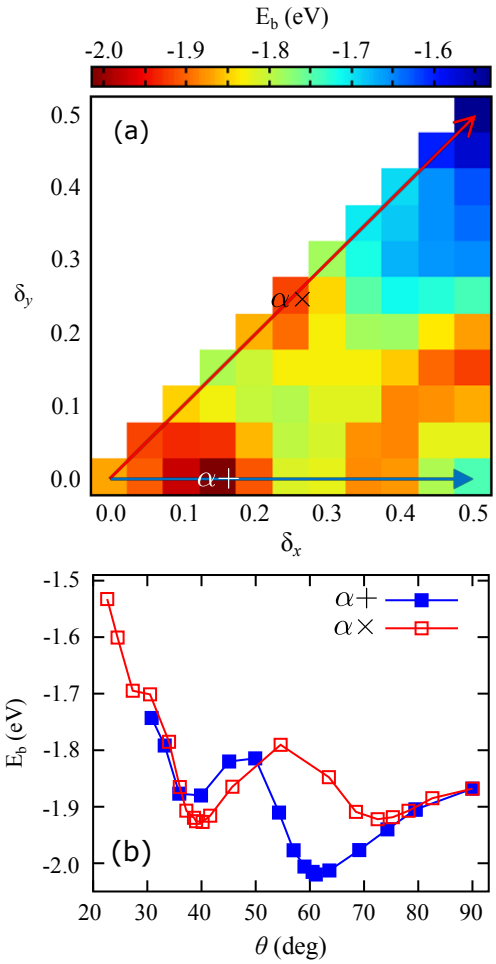

FIG. 2. Binding energy E_b of bilayer poly-MnPc as a function of (a) relative shift in fractional units between the two MnPc layers and (b) stacking angle θ.

Next, we examine how the above-mentioned structural distortion affects the local electronic structure of Mn atoms. For this purpose, we compare the spin-dependent projected density of states (PDOS) of $3d$ orbitals of a Mn atom between monolayer and bilayer poly-MnPc. The PDOS of d_{xy} and $d_{x^2-y^2}$ orbitals for bilayer poly-MnPc are almost the same as those for monolayer poly-MnPc. Among d_{yz}, d_{xz}, and d_{z^2} orbitals, d_{z^2} orbital has the most significant changes in the PDOS. As shown in Fig. 3a, the spin-up (spin-down) PDOS for monolayer poly-MnPc exhibits a sharp peak at -4.15 (1.06) eV relative to the Fermi level. When the Mn atom moves out of the molecular plane in bilayer poly-MnPc, three notable changes in the PDOS of d_{z^2} orbital occur. 1) The spin-up PDOS peak at -4.15 eV splits into two peaks. The first one is still at around -4.15 eV and the second one is at -3.76 eV. As highlighted in Figs. 3a and 3b, the second PDOS peak is coincident with a PDOS plateau of p_z orbitals of pyrrole N atoms. This evidences that the Mn d_{z^2} orbital is hybridized with the p_z orbitals of pyrrole N atoms. Such a d_{z^2}-p_z hybridization can also be seen from the following two additional notable changes. 2) The spin-down PDOS peak at 1.06 eV splits into several peaks, which spread over a wide energy range. 3) A new PDOS peak occurs at -2.40 eV in the spin-up channel.

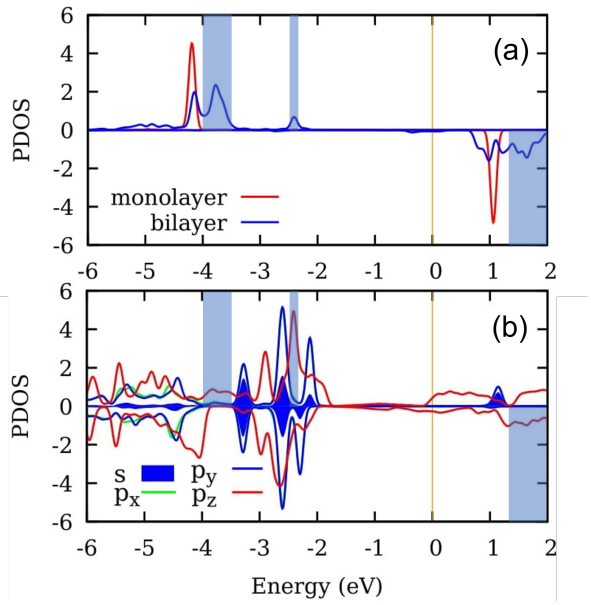

FIG. 3. PDOS of (a) d_{z^2} orbital of a Mn atom for both monolayer and bilayer poly-MnPc and (b) s and p orbitals of the four pyrrole N atoms bonded with the Mn atom for bilayer poly-MnPc. The positive and negative numbers indicate spin-up and spin-down channel respectively. The Fermi level is set to zero.

B. Magnetic Configurations

In this section, we present collinear DFT simulation results for different magnetic configurations in bilayer poly-MnPc. Our calculations are based on a 2×2 supercell

(see Figs. 4a and 4b), which should be large enough for determining the ground-state intralayer magnetic configuration since the 1st and the 2nd nearest neighbor intralayer exchange coupling parameters are dominant [25]. We examine three intralayer magnetic configurations: a ferromagnetic configuration, a Néel antiferromagnetic (NAF) configuration, and a collinear antiferromagnetic (CAF) configuration. In the NAF configuration, all nearest neighbor spins are antiparallel to each other, while in the CAF configuration there are rows of parallel spins, with two adjacent rows antiparallel to each other. The interlayer magnetic ordering we denote a ferromagnetic/antiferromagnetic (FM/AF) configuration if the spin of every Mn atom in one layer is parallel/antiparallel to the spin of the nearest Mn atom in the other layer. Fig. 4a illustrates a magnetic configuration denoted *uddu uddu*, in which u/d stands for spin up/down for a Mn atom, and the first four/last four letters are for the four Mn atoms in the bottom/top layer. In this case, the intralayer magnetic configuration is NAF within both MnPc layers, and the interlayer magnetic configuration is FM. Table I shows DFT total energies for eight magnetic configurations before and after relaxation: In the first set of calculations, we fix lattice constants and atomic positions to be those of the *uuuu uuuu* magnetic configuration, and the resulting energy differences are purely from magnetic interactions. In the second set of calculations, we relax both lattice constants and atomic positions for each magnetic configuration, and the resulting energies, which are those given in parentheses, include contributions from both structural change and magnetic interactions. The energy of the *uddu uddu* configuration in the second set of calculations is overall lowest, and thus set to zero as a reference.

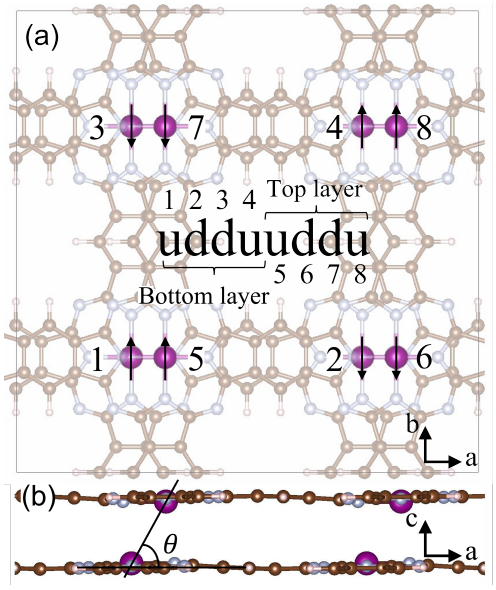

FIG. 4. (a) Top view of the bilayer poly-MnPc with an illustration of the ground-state magnetic configuration *uddu uddu*. (b) Side view of 2×2 supercell.

MC	Intralayer MC	Interlayer MC	E (meV)	M (μ_B)
uddu uddu	NAF-NAF	FM	11 (0)	0.0
uddu duud	NAF-NAF	AF	706 (589)	0.0
udud udud	CAF-CAF	FM	116 (127)	0.0
udud dudu	CAF-CAF	AF	499 (383)	0.0
uudd uudd	CAF-CAF	FM	191 (205)	0.0
uudd dduu	CAF-CAF	AF	465 (357)	0.0
uuuu uuuu	FM-FM	FM	138 (136)	24.9
uuuu dddd	FM-FM	AF	482 (398)	0.0

TABLE I. Total energies and magnetic moments of bilayer poly-MnPc in different magnetic configurations (MCs) The numbers in parentheses are results after structural relaxation.

When bilayer poly-MnPc is in the ground state (*uddu uddu*), each layer is NAF and the whole system is semiconducting with an indirect band gap (see Fig. 5a) of 11 meV. The NAF magnetic configuration of each layer is different from the ground-state magnetic configuration of suspended monolayer poly-MnPc, which is CAF [25]. As such, the interlayer coupling appears to influence the intralayer magnetic state. If we remove one poly-MnPc layer, we find that the remaining poly-MnPc layer (with fixed atomic positions) is metallic in the NAF state (see Fig. 5b). This, surprisingly, indicates that interlayer coupling plays an important role in rendering bilayer poly-MnPc a semiconductor. Our results clearly show that bilayer poly-MnPc differs from monolayer poly-MnPc in both magnetic and electronic properties.

As shown in Fig. 6a, FM bilayer poly-MnPc is metallic. Therefore, bilayer poly-MnPc should undergo a semiconductor-to-metal phase transition when it is subject to an increasing magnetic field. Roughly speaking, the magnetic field required to induce such a phase transition is $94.4\,\mathrm{T} = 136\,\mathrm{meV}/24.9\,\mu_B$, where 136 meV is the energy difference between the FM state and the ground state (per 2×2 supercell) and $24.9\,\mu_B$ is the magnetic moment of the FM state (per 2×2 supercell). Although FM monolayer poly-MnPc is half-metallic [24, 25] (see also Fig. 6b), FM bilayer poly-MnPc is metallic in both spin channels. The spin-up conduction band, which is completely empty in FM monolayer poly-MnPc, becomes partially occupied in the FM bilayer poly-MnPc. As electrons migrate from the spin-down channel to the spin-up channel, the imbalance between the two spin channels increases. Consequently, the average magnetic moment per Mn atom increases from $3.0\,\mu_B$ to $3.1 \approx 24.9/8\,\mu_B$.

C. Magnetic Coupling Constants

From the DFT energies of different magnetic configurations, we estimate exchange coupling constants using a phenomenological Heisenberg model with spins

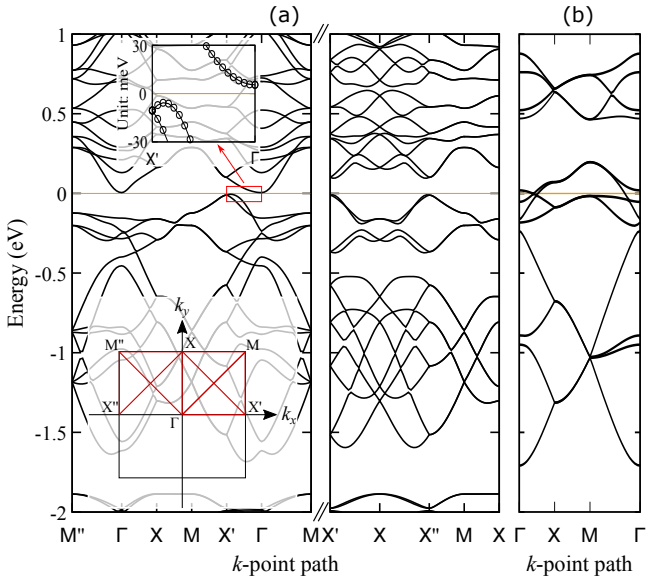

FIG. 5. Band Structure of (a) bilayer poly-MnPc in the ground state with the *uddu uddu* magnetic configuration and (b) monolayer poly-MnPc (taken from the bilayer poly-MnPc without further relaxation) with the *uddu* magnetic configuration. The spin-up energy bands are identical to the spin-down energy bands. The zoomed-in upper inset in panel (a) shows an indirect band gap. The lower inset in panel (a) illustrates the k-point path.

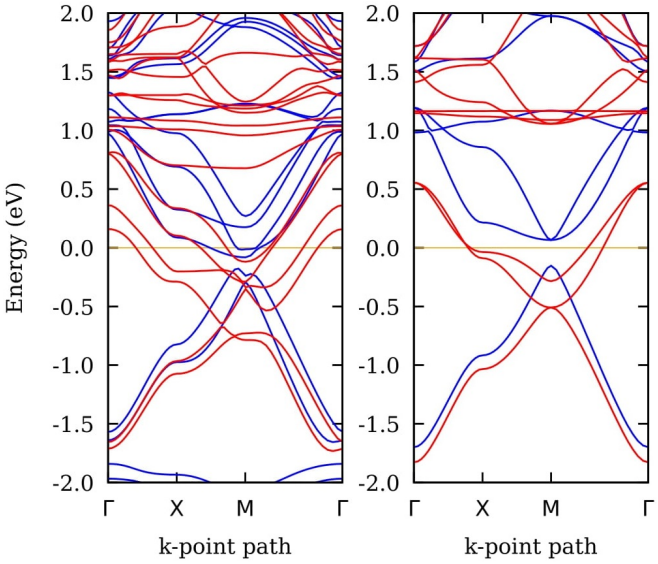

FIG. 6. Band structures of (a) bilayer and (b) monolayer poly-MnPc in the ferromagnetic state. The blue line represents the spin-up bands and red indicates the spin-down bands. The Fermi level is set to zero.

treated classically. The model Hamiltonian is given by $H = H_{\text{intra}} + H_{\text{inter}}$, where H_{inter} contains the interactions among Mn atoms within a layer and H_{inter} the magnetic interaction between different layers,

$$H_{\text{intra}} = \frac{1}{2}\left(J_1 \sum_{\langle ij\rangle_x^1} S_i S_j + J_2 \sum_{\langle ij\rangle_y^1} S_i S_j + J_3 \sum_{\langle ij\rangle^2} S_i S_j \right), \tag{1}$$

$$H_{\text{inter}} = \frac{1}{2}\left(J_4 \sum_{\langle ij\rangle^1} S_i S_j + J_5 \sum_{\langle ij\rangle^2} S_i S_j + J_6 \sum_{\langle ij\rangle^3} S_i S_j + J_7 \sum_{\langle ij\rangle^4} S_i S_j \right). \tag{2}$$

J_1 through J_3 thus characterize intralayer couplings and J_4 through J_7 represent interlayer couplings. $\langle ij\rangle^n$ denotes that site i is the nth nearest neighbor of site j. The rank n of nth nearest neighbor is determined separately within a layer and between different layers. $\langle ij\rangle_{x/y}^1$ denotes that the two sites are nearest neighbors along the x/y direction. Due to the relative shift along the x-direction between two poly-MnPc layers, we introduce two separate exchange coupling constants for the nearest neighbor intralayer interaction, namely J_1 along the x-direction and J_2 along the y-direction. The pairs of Mn atoms for each exchange coupling constant are tabulated in Table II together with the corresponding Mn-Mn distance.

Coupling	Coupling Pairs	L (Å)	Value (meV)
J_1	{1,2},{3,4},{5,6},{7,8}	10.64	−0.77 (-0.05)
J_2	{1,3},{2,4},{5,7},{6,8}	10.64	−1.92 (−1.50)
J_3	{1,4},{2,3},{5,8},{6,7}	15.05	0.91 (0.71)
J_4	{1,5},{2,6},{3,7},{4,8}	3.21	−23.55 (−17.5)
J_5	{1,6},{2,5},{3,8},{4,7}	9.51	6.40 (5.98)
J_6	{1,7},{2,8},{3,5},{4,6}	11.11	3.34 (3.11)
J_7	{1,8},{2,7},{3,6},{4,5}	14.27	−5.29 (−6.14)

TABLE II. Fit exchange coupling constants of the phenomenological classical Heisenberg model. The indices of eight Mn atoms are defined in Fig. 4a. L is the separation between two Mn atoms. The numbers in parentheses are results after structural relaxation.

Using the magnetic configurations presented in Section III B, we set up eight linear equations to solve the seven exchange coupling constants and an additional energy constant which is not due to exchange interaction. The calculated exchange coupling constants are given in Table II. The interlayer exchange couplings J_4 to J_7 are stronger than the intralayer exchange couplings J_1 to J_3. The nearest-neighbor interlayer coupling constant J_4 is largest in magnitude, and its negative sign signifies ferromagnetic coupling. J_2 is the strongest intralayer coupling constant, and it is more than a factor of 10 times smaller than J_4 in magnitude. J_1 differs from J_2, which manifests the broken symmetry due to the relative shift between the two poly-MnPc layers.

We also simulated bilayer molecular MnPc in the atomic structure reported by Yamada *et al.* [29] using a rhombic unit cell with lattice constants of 17.6 Å and

82°. The interlayer stacking in bilayer molecular MnPc is also $\alpha+$ [46], and the stacking angle is 60.7° (63.7°) in the FM (AFM) state after structural relaxation. According to our calculations, the FM state is 182 meV lower in energy than the AFM state with each state in its relaxed structure, and the intralayer exchange coupling constants are less than 2 μeV. The interlayer exchange coupling constant is −63.46 meV with fixed atomic positions which are relaxed in the FM configuration (the ground state). This reduces to −40.39 meV if we further relax the atomic positions for the AFM magnetic configuration. These results are close to previous DFT findings [46]. However, our calculated interlayer exchange coupling constant for bilayer molecular MnPc is much larger than the experimental value ($\sim$ 1 meV) for molecular crystals of MnPc. [47]. It is not known if such a difference is due to reduction in the length of the Mn chain, and further studies are needed to explain this.

One related observation in our calculations is that certain d-orbital occupation matrix elements differ significantly between the (interlayer) FM and AFM states. It is noteworthy that such differences are stabilized by structural relaxation for both FM and AFM states. For example, Eq. (3) and Eq. (4) show the spin-down d-orbital occupation matrix $D^{\downarrow}_{\rm FM}$ ($D^{\downarrow}_{\rm AFM}$) of Mn atoms of bilayer molecular MnPc FM and AFM configurations,

$$D^{\downarrow}_{\rm FM} = \begin{pmatrix} 0.06 & 0.00 & 0.00 & 0.00 & 0.08 \\ 0.00 & 0.16 & 0.01 & 0.00 & 0.00 \\ 0.00 & 0.01 & 0.10 & 0.07 & -0.01 \\ 0.00 & 0.00 & 0.07 & 0.17 & -0.01 \\ 0.08 & 0.00 & -0.01 & -0.01 & 0.32 \end{pmatrix} \quad (3)$$

$$D^{\downarrow}_{\rm AFM} = \begin{pmatrix} 0.06 & 0.00 & 0.00 & 0.00 & 0.08 \\ 0.00 & 0.35 & 0.00 & -0.04 & 0.00 \\ 0.00 & 0.00 & 0.06 & 0.00 & -0.01 \\ 0.00 & -0.04 & 0.00 & 0.06 & 0.00 \\ 0.08 & 0.00 & -0.01 & 0.00 & 0.32 \end{pmatrix} \quad (4)$$

The d orbitals in the occupation matrix are in the order d_{xy}, d_{yz}, d_{z^2}, d_{xz}, and $d_{x^2-y^2}$. As highlighted in Eqs. (3(and (4), the diagonal matrix element corresponding to the d_{yz} (d_{xz}) orbital changes by as much as 0.19 (0.11). In comparison, the change in the d-orbital occupation matrix elements is no larger than 0.05 for bilayer poly-MnPc as the magnetic configuration changes from *uddu uddu* to *uddu duud*. As such, the large value of the calculated exchange coupling constant seems to be correlated with changes in the d-orbital occupation matrix.

D. Magnetic Coupling Pathway

We report here the dominant coupling pathway between layers based on Wannier analysis using a 1 × 1 unit cell. The inner and outer energy windows were respectively set to $[-1.74 : 0.19]$ eV and $[-1.74 : 1.00]$ eV relative to the Fermi level. We obtained four Wannier functions since there are four energy bands in the inner energy window. As shown in Figs. 7a–7d, the Wannier functions extend along the $-a$, $+a$, $-b$, and $+b$ directions respectively. The first (last) two Wannier functions exhibit anti-bonding (bonding) between the organic part of the two layers. There is no evidence of direct interlayer coupling via neighboring Mn atoms.

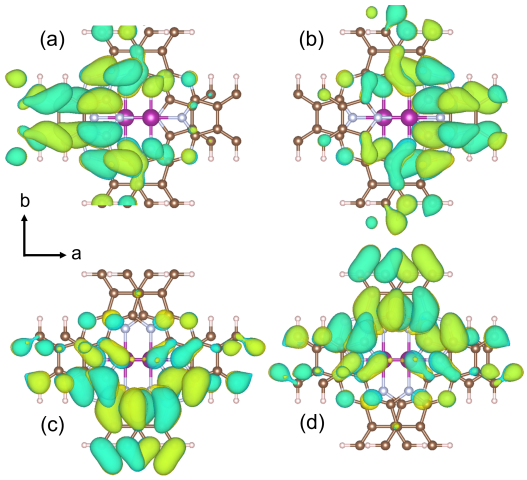

FIG. 7. Four Wannier functions below the Fermi level. The isosurface value is ± 2 Å$^{-3/2}$. Yellow is for positive values and cyan for negative values.

To reveal more details of the interlayer coupling, we examine three cross sections of the Wannier function in Fig. 7a using colormap. As seen from the colormap in Fig. 8, there is strong hybridization between d orbitals of Mn atoms and π orbitals from surrounding N and C atoms; and the interlayer coupling is mainly through the π orbitals of C and N atoms. Such observations are valid for the other three Wannier functions as well. It is noteworthy that the d orbitals of Mn atoms are anti-bonding with the π orbitals for all the four Wannier functions.

IV. MAGNETIC ANISOTROPY ENERGY

Finally, we examine the magnetic anisotropy energy of FM bilayer poly-MnPc using a 1 × 1 unit cell. Fig. 9 shows the energy difference $\Delta E = [E(\theta) - E(\theta = 0°)]/2$, where $E(\theta)$ is the DFT energy as a function of polar angle θ of the local spins. The azimuthal angle ϕ is fixed at zero. The local spins are perpendicular to (parallel with) the molecular plane when $\theta = 0°/180°$ ($\theta = 90°$). The factor of 2 in the denominator is the number of Mn atoms in a unit cell. Note that the two Mn atoms contribute equally to spin orbit coupling (SOC) energy. The system has its lowest (highest) energy when θ is around 0°/180° (90°). Due to the asymmetric structure along the z direction, the values of ΔE are slightly higher with polar angles less than 90° than the values with the angles beyond 90°. The magnetic anisotropy energy MAE is about 1.0 meV ($\Delta E(\theta = 85°)$). At $\theta = 90°$, we rotate the spins by varying ϕ with steps of 30° and find that

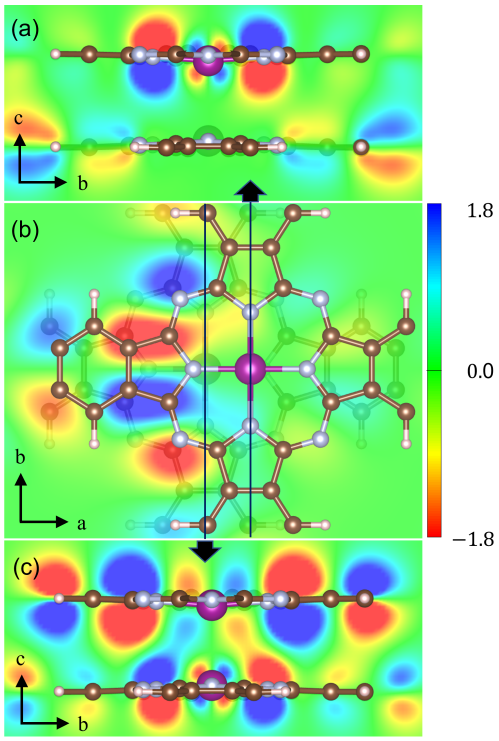

FIG. 8. Cross-sectional images of the same Wannier function with a Mn atom of (a) the top layer and (c) the bottom layer. (b) The cross-sectional image is between the two poly-MnPc layers. Units for the colorbar scale are $Å^{-3/2}$.

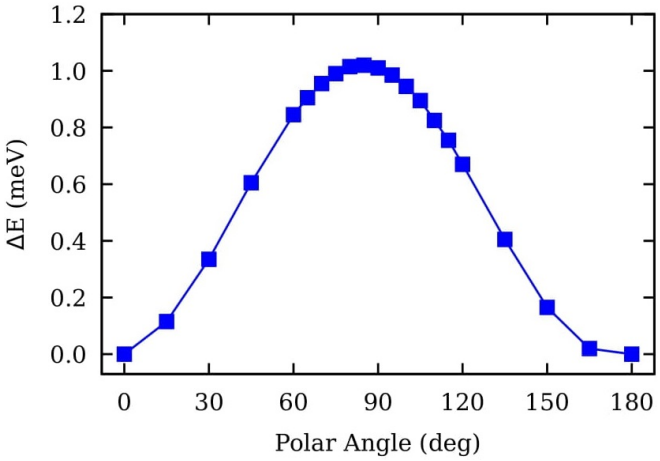

FIG. 9. Relative energy per Mn atom versus the direction of spins for FM bilayer poly-MnPc in a 1×1 unit cell.

the change in energy is smaller than $40\,\mu$eV: the system has a magnetic easy axis almost perpendicular to the molecular plane, and the in-plane magnetic anisotropy is negligibly small. The total orbital moment of each Mn atom at $(\theta = 0°, \phi = 0°)$ is $0.007\,\mu_B$.

V. CONCLUSION AND DISCUSSION

In this work, we performed DFT studies of bilayer MnPc molecules and polymeric sheets. We found that in the ground state there is a relative shift of the top layer by $\sim 1/8$ of the x-axis lattice vector with respect to the bottom layer with a stacking angle of 61.1° in the $\alpha+$ stacking model. In the ground state, bilayer poly-MnPc is an indirect band gap semiconductor with ferromagnetic interlayer magnetic ordering and Néel antiferromagnetic magnetic ordering in each layer. The indirect band gap is 11 meV. In the ferromagnetic state, which is 136 meV higher in energy, bilayer poly-MnPc is a normal metal with enhanced average magnetic moment per Mn atom ($3.1\,\mu_B$). We found that interlayer exchange couplings are much stronger than intralayer exchange couplings. According to our Wannier analysis, the strongest inter-layer magnetic coupling path is via π orbitals of surrounding carbon atoms. In bilayer MnPc molecules, we reveal a strong dependence of d-orbital occupation on the interlayer magnetic configuration. Compared with bilayer polymeric MnPc, a bigger change in the d-orbital occupation results in stronger interlayer exchange coupling in bilayer molecular MnPc. Mn atoms move out of the molecular plane in bilayer poly-MnPc resulting in hybridization between d_{z^2} orbitals of Mn atoms and p_z orbitals of the surrounding N atoms. The magnetic anisotropy was investigated for bilayer poly-MnPc, showing that the easy axis is almost perpendicular to the molecular plane with a magnetic anisotropy energy of 1.0 meV per Mn atom.

ACKNOWLEDGMENTS

This work is supported by US DOE/BES EFRC program with award No. DE-SC0019330. J.N.F. acknowledges US DOE/BES grant No. DE-FG02-02ER45995. Computations were done using the utilities of the National Energy Research Scientific Computing Center and University of Florida Research Computing.

[1] K. S. Novoselov, A. K. Geim, S. V. Morozov, D. Jiang, Y. Zhang, S. V. Dubonos, I. V. Grigorieva, and A. A. Firsov, Science **306**, 666 (2004).
[2] H. Liu, A. T. Neal, Z. Zhu, Z. Luo, X. Xu, D. Tománek, and P. D. Ye, ACS Nano **8**, 4033 (2014).
[3] S. Das, W. Zhang, M. Demarteau, A. Hoffmann, M. Dubey, and A. Roelofs, Nano Letters **14**, 5733 (2014).
[4] K. F. Mak, C. Lee, J. Hone, J. Shan, and T. F. Heinz, Physical Review Letters **105**, 136805 (2010).
[5] J. R. Schaibley, H. Yu, G. Clark, P. Rivera, J. S. Ross, K. L. Seyler, W. Yao, and X. Xu, Nature Reviews Materials **1**, 16055 (2016).
[6] J.-G. Park, Journal of Physics: Condensed Matter **28**, 301001 (2016).

[7] K. S. Burch, D. Mandrus, and J.-G. Park, Nature **563**, 47 (2018).
[8] B. Dieny and M. Chshiev, Reviews of Modern Physics **89**, 025008 (2017).
[9] B. Tudu and A. Tiwari, Vacuum **146**, 329 (2017).
[10] J.-X. Yu and J. Zang, Science Advances **4**, eaar7814 (2018).
[11] T. Song, Z. Fei, M. Yankowitz, Z. Lin, Q. Jiang, K. Hwangbo, Q. Zhang, B. Sun, T. Taniguchi, K. Watanabe, M. A. McGuire, D. Graf, T. Cao, J.-H. Chu, D. H. Cobden, C. R. Dean, D. Xiao, and X. Xu, Nature Materials **18**, 1298 (2019).
[12] E. C. Ahn, npj 2D Materials and Applications **4**, 17 (2020).
[13] J. L. Lado and J. Fernández-Rossier, 2D Materials **4**, 035002 (2017).
[14] B. Huang, G. Clark, D. R. Klein, D. MacNeill, E. Navarro-Moratalla, K. L. Seyler, N. Wilson, M. A. McGuire, D. H. Cobden, D. Xiao, W. Yao, P. Jarillo-Herrero, and X. Xu, Nature Nanotechnology **13**, 544 (2018).
[15] M. Bonilla, S. Kolekar, Y. Ma, H. C. Diaz, V. Kalappattil, R. Das, T. Eggers, H. R. Gutierrez, M.-H. Phan, and M. Batzill, Nature Nanotechnology **13**, 289 (2018).
[16] D. J. O'Hara, T. Zhu, A. H. Trout, A. S. Ahmed, Y. K. Luo, C. H. Lee, M. R. Brenner, S. Rajan, J. A. Gupta, D. W. McComb, and R. K. Kawakami, Nano Letters **18**, 3125 (2018).
[17] Y. Deng, Y. Yu, Y. Song, J. Zhang, N. Z. Wang, Z. Sun, Y. Yi, Y. Z. Wu, S. Wu, J. Zhu, J. Wang, X. H. Chen, and Y. Zhang, Nature **563**, 94 (2018).
[18] W. Wu, A. Kerridge, A. H. Harker, and A. J. Fisher, Physical Review B **77**, 184403 (2008).
[19] C. Gong, L. Li, Z. Li, H. Ji, A. Stern, Y. Xia, T. Cao, W. Bao, C. Wang, Y. Wang, Z. Q. Qiu, R. J. Cava, S. G. Louie, J. Xia, and X. Zhang, Nature **546**, 265 (2017).
[20] B. Huang, G. Clark, E. Navarro-Moratalla, D. R. Klein, R. Cheng, K. L. Seyler, D. Zhong, E. Schmidgall, M. A. McGuire, D. H. Cobden, W. Yao, D. Xiao, P. Jarillo-Herrero, and X. Xu, Nature **546**, 270 (2017).
[21] M. Gakiya-Teruya, X. Jiang, D. Le, O. Üngör, A. J. Durrani, J. J. Koptur-Palenchar, J. Jiang, T. Jiang, M. W. Meisel, H.-P. Cheng, X.-G. Zhang, X.-X. Zhang, T. S. Rahman, A. F. Hebard, and M. Shatruk, Journal of the American Chemical Society **143**, 14563 (2021).
[22] S. Heutz, C. Mitra, W. Wu, A. Fisher, A. Kerridge, M. Stoneham, A. H. Harker, J. Gardener, H.-H. Tseng, T. Jones, C. Renner, and G. Aeppli, Advanced Materials **19**, 3618 (2007).
[23] M. Koudia and M. Abel, Chem. Commun. **50**, 8565 (2014).
[24] J. Zhou and Q. Sun, Journal of the American Chemical Society **133**, 15113 (2011).
[25] Y.-P. Wang, X.-G. Li, S.-L. Liu, J. N. Fry, and H.-P. Cheng, Phys. Rev. B **97**, 115419 (2018).
[26] C. J. Benjamin, S. K. Zhang, and Z. H. Chen, Nanoscale **10**, 5148 (2018).
[27] N. M. Vargas, F. Torres, A. A. Baker, J. R. I. Lee, M. Kiwi, T. M. Willey, C. Monton, and I. K. Schuller, Applied Physics Letters **117**, 6 (2020).
[28] M. Studniarek, S. Cherifi-Hertel, E. Urbain, U. Halisdemir, R. Arras, B. Taudul, F. Schleicher, M. Herve, C. H. Lambert, A. Hamadeh, L. Joly, F. Scheurer, G. Schmerber, V. Da Costa, B. Warot-Fonrose, C. Marcelot, O. Mauguin, L. Largeau, F. Leduc, F. Choueikani, E. Otero, W. Wulfhekel, J. Arabski, P. Ohresser, W. Weber, E. Beaurepaire, S. Boukari, and M. Bowen, Advanced Functional Materials **27**, 5 (2017).
[29] H. Yamada, T. Shimada, and A. Koma, The Journal of Chemical Physics **108**, 10256 (1998).
[30] S. Sanvito, Nature Physics **6**, 562 (2010).
[31] M. Cinchetti, V. A. Dediu, and L. E. Hueso, Nature Materials **16**, 507 (2017).
[32] F. Djeghloul, F. Ibrahim, M. Cantoni, M. Bowen, L. Joly, S. Boukari, P. Ohresser, F. Bertran, P. L. Fèvre, P. Thakur, F. Scheurer, T. Miyamachi, R. Mattana, P. Seneor, A. Jaafar, C. Rinaldi, S. Javaid, J. Arabski, J. P. Kappler, W. Wulfhekel, N. B. Brookes, R. Bertacco, A. Taleb-Ibrahimi, M. Alouani, E. Beaurepaire, and W. Weber, Scientific Reports **3**, 1272 (2013).
[33] J. Girovsky, J. Nowakowski, M. E. Ali, M. Baljozovic, H. R. Rossmann, T. Nijs, E. A. Aeby, S. Nowakowska, D. Siewert, G. Srivastava, C. Wäckerlin, J. Dreiser, S. Decurtins, S.-X. Liu, P. M. Oppeneer, T. A. Jung, and N. Ballav, Nature Communications **8**, 15388 (2017).
[34] C. G. Barraclough, R. L. Martin, S. Mitra, and R. C. Sherwood, The Journal of Chemical Physics **53**, 1638 (1970).
[35] P. Hohenberg and W. Kohn, Physical Review **136**, B864 (1964).
[36] W. Kohn and L. J. Sham, Physical Review **140**, A1133 (1965).
[37] G. Kresse and J. Hafner, Physical Review B **47**, 558 (1993).
[38] G. Kresse and D. Joubert, Physical Review B **59**, 1758 (1999).
[39] H. J. Monkhorst and J. D. Pack, Physical Review B **13**, 5188 (1976).
[40] J. Klimes, D. R. Bowler, and A. Michaelides, Physical Review B **83**, 195131 (2011).
[41] P. E. Blochl, Physical Review B **50**, 17953 (1994).
[42] A. I. Liechtenstein, V. I. Anisimov, and J. Zaanen, Physical Review B **52**, R5467 (1995).
[43] N. Marzari and D. Vanderbilt, Physical Review B **56**, 12847 (1997).
[44] I. Souza, N. Marzari, and D. Vanderbilt, Phys. Rev. B **65**, 035109 (2001).
[45] A. A. Mostofi, J. R. Yates, Y.-S. Lee, I. Souza, D. Vanderbilt, and N. Marzari, Computer Physics Communications **178**, 685 (2008).
[46] B. Brena, B. Sanyal, and H. C. Herper, The Journal of Physical Chemistry C **124**, 27185 (2020).
[47] C. G. Barraclough, A. K. Gregson, and S. Mitra, The Journal of Chemical Physics **60**, 962 (1974).